International Journal of Nanomedicine

Dovepress
open access to scientific and medical research

Open Access Full Text Article

ORIGINAL RESEARCH

Green Synthesis of Fe_3O_4 Nanoparticles Stabilized by a *Garcinia mangostana* Fruit Peel Extract for Hyperthermia and Anticancer Activities

This article was published in the following Dove Press journal:
International Journal of Nanomedicine

Mostafa Yusefi[1]
Kamyar Shameli[1]
Ong Su Yee[1]
Sin-Yeang Teow[2]
Ziba Hedayatnasab[3,4]
Hossein Jahangirian[5]
Thomas J Webster[5]
Kamil Kuča[1,6]

[1]Department of Chemical and Environmental Engineering, Malaysia-Japan International Institute of Technology, Universiti Teknologi Malaysia, Kuala Lumpur, 54100, Malaysia; [2]Department of Medical Sciences, School of Medical and Life Sciences, Sunway University, Petaling Jaya, Selangor Darul Ehsan, 47500, Malaysia; [3]Department of Chemical Engineering, Faculty of Engineering, University of Malaya, Kuala Lumpur, 50603, Malaysia; [4]Department of Chemical and Petroleum Engineering, Sharif University of Technology, Tehran, 11155-9465, Iran; [5]Department of Chemical Engineering, College of Engineering, Northeastern University, Boston, MA, 02115, USA; [6]Department of Chemistry, Faculty of Science, University of Hradec Kralove, Hradec Kralove, Czech Republic

Introduction: Fe_3O_4 nanoparticles (Fe_3O_4 NPs) with multiple functionalities are intriguing candidates for various biomedical applications.

Materials and Methods: This study introduced a simple and green synthesis of Fe_3O_4 NPs using a low-cost stabilizer of plant waste extract rich in polyphenols content with a well-known antioxidant property as well as anticancer ability to eliminate colon cancer cells. Herein, Fe_3O_4 NPs were fabricated via a facile co-precipitation method using the crude extract of *Garcinia mangostana* fruit peel as a green stabilizer at different weight percentages (1, 2, 5, and 10 wt.%). The samples were analyzed for magnetic hyperthermia and then in vitro cytotoxicity assay was performed.

Results: The XRD planes of the samples were corresponding to the standard magnetite Fe_3O_4 with high crystallinity. From TEM analysis, the green synthesized NPs were spherical with an average size of 13.42±1.58 nm and displayed diffraction rings of the Fe_3O_4 phase, which was in good agreement with the obtained XRD results. FESEM images showed that the extract covered the surface of the Fe_3O_4 NPs well. The magnetization values for the magnetite samples were ranging from 49.80 emu/g to 69.42 emu/g. FTIR analysis verified the functional groups of the extract compounds and their interactions with the NPs. Based on DLS results, the hydrodynamic sizes of the Fe_3O_4 nanofluids were below 177 nm. Furthermore, the nanofluids indicated the zeta potential values up to −34.92±1.26 mV and remained stable during four weeks of storage, showing that the extract favorably improved the colloidal stability of the Fe_3O_4 NPs. In the hyperthermia experiment, the magnetic nanofluids showed the acceptable specific absorption rate (SAR) values and thermosensitive performances under exposure of various alternating magnetic fields. From results of in vitro cytotoxicity assay, the killing effects of the synthesized samples against HCT116 colon cancer cells were mostly higher compared to those against CCD112 colon normal cells. Remarkably, the Fe_3O_4 NPs containing 10 wt.% of the extract showed a lower IC_{50} value (99.80 µg/mL) in HCT116 colon cancer cell line than in CCD112 colon normal cell line (140.80 µg/mL).

Discussion: This research, therefore, introduced a new stabilizer of *Garcinia mangostana* fruit peel extract for the biosynthesis of Fe_3O_4 NPs with desirable physiochemical properties for potential magnetic hyperthermia and colon cancer treatment.

Keywords: green synthesis, Fe_3O_4 nanoparticles, *Garcinia mangostana*, magnetic hyperthermia, cytotoxicity assay

Introduction

Fe_3O_4 nanoparticles (Fe_3O_4 NPs) can play an important role in cancer therapy. Fabrication of Fe_3O_4 NPs can be carried out by different procedures such as co-precipitation, thermal decomposition, and green synthesis.[1–3] Co-precipitation is

Correspondence: Kamyar Shameli; Kamil Kuča
Email kamyarshameli@gmail.com; kamil.kuca@uhk.cz

a conventional method withthe capability to produce large-scale of Fe_3O_4 NPs.[4–6] This method still requires improvement particularly in controlling the particle size and composition of the NPs. In synthesis of Fe_3O_4 NPs, different types of natural stabilizers such as plant extracts and bioactive molecules can increase the colloidal stability and physiochemical characteristic of Fe_3O_4 NPs.[1,7–9] It has been reported that coating the NPs could be costly, laborious, time-consuming, and toxic to the environment when chemicals are used.[10] To overcome these issues, preparation of NPs by a green approach has drawn considerable attention.[11] During the green synthesis process, natural-based stabilizers may hydrolyze iron salt solution for ferric hydroxide formation, which is then reduced by biomolecules to form NPs.[12] As a green stabilizer, plant extracts and its polyphenolic compounds could be presented into/onto NPs to decrease particle interactions as well as improve thermodynamic stability.[1,13] Therefore, Fe_3O_4 NPs stabilized with the plant extracts could potentially show better water permeability, antioxidant activity, biocompatibility, biodegradability, and tolerable toxicity for various biomedical applications compared to using other traditional methods.[14–16]

Compared to the normal amount consumed with a low phenolic content, the plant extract might induce a greater amount of a metabolite compound of polyphenol or flavonoid subclass and distribute at the targeted site for stronger antioxidant and anticancer activities.[17] Polyphenols, especially anthocyanins, undergo a major structural changes during the in vitro or in vivo evaluations, improving both bioavailability and biological properties.[18] It is worth mentioning that the peel of some fruits has higher antioxidant activities than the pulp.[19] The extract of fruit peels such as *Garcinia mangostana* (*G. mangostana*)[19] and mango[20] are rich sources of antioxidants. Even though there are many studies related to the green synthesis of Fe_3O_4 NPs using different plant extracts such as *Kappaphycus alvarezii*[21] and *Punica granatum* peel;[6] however, applications of the green synthesized Fe_3O_4 NPs with anticancer properties are still less focused.[1]

Over the years, using agro-waste has been intriguing for researchers to fabricate environmental-friendly materials to tackle problems of toxicity and the reduction in landfill space.[22] *G. mangostana* is known as mangosteen and considered as a tropical fruit from Guttiferea family. It contains 17% outer pericarp, 48% inner pericarp, 31% juicy flesh, and 4% cap.[23] The pulp extract of *G. mangostana* has been famously used for a food supplement and herbal medicine.[19] Peel of *G. mangostana* is considered as a waste material, albeit, its crude extract may contain benzophenones, flavonoids, and anthocyanins compounds with antioxidant properties.[24] For example, xanthones in flavonoid compounds with a high composition of α-mangostin and γ-mangostin have been reported for anticancer treatments.[24] Xanthones have been used to treat different types of cancer cells.[25] Despite that there have been some studies on *G. mangostana* fruit peels in synthesis of Au NPs[26] and Ag NPs,[27] there have been no precise studies on the ability of *G. mangostana* to synthesize Fe_3O_4 NPs.

Magnetic hyperthermia therapy (MHT) is currently considered as an attractive application of Fe_3O_4 NPs in cancer treatment, however, it is still under the clinical trial.[28] For this purpose, the ferrofluid samples are exposed to an external alternating magnetic field (AMF) in order to assess their heating capabilities known as specific absorption rate (SAR). In MHT, the AMF strengths can control the hyperthermia temperature (T_H) and properties of Fe_3O_4 NPs.[29] It has been stated that a secure T_H is ranged from 42°C to 47°C to cause hydrolyzing the tissue's proteins and acute necrotic cancer cell death over 30–60 min, whereas the normal cells can be unaffected due to heat transfer phenomena.[28,30] It is worth mentioning that Fe_3O_4 NPs in a low-viscous medium may trigger a magnetic response of anisotropic particles to be physically rotated by Brownian heating loss mechanism for increments of T_H and SAR values.[31] This may be achieved by developing the green synthesis of Fe_3O_4 NPs stabilized with a plant extract.

Based on World Health Organization (WHO) report, there have been approximately 18 million cancer cases and nearly 9.6 million people have died of cancer in the year 2018 alone.[32] In nanomedicine, NPs smaller than 10 nm are likely to be removed through renal clearance, whereas NPs bigger than 100 nm can be trapped rapidly in spleen and liver via macrophage phagocytosis.[33] Fe_3O_4 NPs with an appropriate size and surface chemistry can be applied for various therapeutic applications, including drug delivery, magnetic resonance imaging (MRI) contrast agent and MHT.[1,34–37] There have been studies using co-precipitation method to synthesize Fe_3O_4 NPs for colon cancer treatment.[6,11,16,21] For instance, dextran-coated Fe_3O_4 NPs were synthesized by using a facile co-precipitation method with a mean size of ~10 nm.[38]

To our best knowledge, this current study is probably the first report to use the crude extract of *G. mangostana* fruit peel as a novel and green stabilizer in the biosynthesis of Fe_3O_4 nanofluids with high quality and low-cost for potential hyperthermia and colon cancer treatments. The Fe_3O_4 NPs

samples were stabilized with various weight percentages of the peel extract and they were evaluated by X-ray powder diffraction (XRD), transmission electron microscopy (TEM), field emission electron microscope (FESEM), energy-dispersive X-ray spectroscopy (EDS), vibrating sample magnetometer (VSM), and Fourier-transform infrared spectroscopy (FTIR). Dynamic light scattering (DLS) was also used to examine the stability of the samples solutions over four weeks of storage. The green synthesized Fe_3O_4 NPs were assessed by magnetic hyperthermia analysis. In addition, the in vitro cytotoxicity assays of the samples were evaluated using the human colon cancer cell line (HCT116) and colon normal cell line (CCD112).

Materials and Methods

Materials

G. mangostana fruit was obtained from Terengganu, Malaysia. Iron (II) chloride tetrahydrate ($FeCl_2.4H_2O \geq 99\%$) and iron (III) chloride hexahydrate ($FeCl_3.6H_2O$, 97%) were purchased from Sigma-Aldrich. Sodium hydroxide (NaOH) was purchased from R&M Chemicals. All aqueous solutions were prepared using double distilled water. The chemicals were used without further purification. All glassware used was washed with distilled water and dried before used.

Preparation of *Garcinia mangostana* Fruit Peel Extract

The extract of *G. mangostana* fruit peel was obtained using a modified method from our group.[6,26] Briefly, the fruit peels were washed several times to remove dust, followed by drying at an ambient condition. A total of 10 g of the fruit peel was ground and mixed with 100 mL double deionized water at 80°C, using an oil bath under a constant stirring at 250 rpm for 1 h. The crude extract solution (10 m/V) was filtered with filter paper (Fioroni 601) and oven-dried at 45°C for 24 h. The dried extract powder was termed as S5 and stored at 4°C for further processing.

Green Synthesis of Fe_3O_4 NPs Stabilized by the Extract of *Garcinia mangostana* Fruit Peel

A simple co-precipitation method and the extract of *G. mangostana* fruit peel as a novel stabilizing and capping agent were used to synthesize Fe_3O_4 NPs. The crude extract of *G. mangostana* fruit peel, iron salts, and sodium hydroxide acted as a stabilizer, iron sources, and a reducing agent, respectively.[6] Four different extract solutions (wt.%) were prepared. In total, 1, 2, 5, and 10 g of the dried extract powder were added into four different beakers containing respectively 99, 98, 95, and 90 g of double deionized water and stirred for 15 min at room temperature. $FeCl_3.6H_2O$, 97% (2.53 g) and $FeCl_2.4H_2O \geq 99\%$ (0.99 g) at a molar ratio of 2:1 were respectively added into each solution. After that, NaOH (1 M) was dropwise added into the respective solutions to adjust the pH to ~11 followed by vigorous stirring for another 30 min. Finally, the samples were centrifuged three times at 14,000 rpm for 12 min and the collected precipitates were oven-dried at 70°C. The same procedure without using the extract was carried out for the preparation of bare Fe_3O_4 NPs. The synthesized Fe_3O_4 NPs with 0, 1, 2, 5, and 10 wt.% concentrations of the peel extract were termed as S0, S1, S2, S3, and S4, respectively, and the peel extract powder alone was termed as S5.

Characterization

The structural characteristics of the synthesized samples (~3 g) were analyzed by using a PANalytical X'Pert PRO XRD with Cu Kα radiation (λ= 0.15406nm). An applied current of 20 mA and an accelerating voltage of 45 kV in a 2θ (from 5° to 80°) with a scanning rate of 2θ/min were used. TEM (JEM-2100F-Japan) determined morphology, particle size, and structure of the sample as the solution of the sample (~1.5 mg in 10 mL distilled water) was dropped onto 300-mesh copper grids and also a TEM image was analyzed under the microscope. FESEM was used to determine the size distribution and morphology of the samples (~2 mg) by using a JSM-7800F Prime Schottky, then the FESEM attached to EDS analysis for chemical characterization of the samples. An accelerating voltage of the microscope was set at 5.0 kV and the standard magnification was selected at 40 kX. Moreover, VSM (Model 7400, Tokyo, Japan) was used to evaluate the magnetic properties of the samples (~2 g) at room temperature. The functional groups of the samples were identified by using IR Tracer-100 FTIR (Thermo Nicolet, USA) within the wavelength range of 400–4000 cm^{-1}. Each sample (~5 mg) was mixed with powder of potassium bromide (KBr) (500 mg) at a ratio of 1:100 w/w to produce a pellet.

Dynamic Light Scattering (DLS) Analysis and Impact of Storage Time on Fe_3O_4 Nanofluids

For DLS analysis, Anton Paar instrument was used to potentially measure stability of the synthesized samples

in the distilled water solution. In order to evaluate the effect of storage time on the Fe_3O_4 NPs dispersions, each sample solution (80 mL; 100 µg/mL) was distributed into four glass bottles (15 mL each), covered with aluminum foil and stored at 4°C.[39–41] Zeta potential, hydrodynamic particle size, and polydispersity index were measured immediately post-synthesis (as prepared) and subsequently after 1, 2, 3, and 4 weeks of storage. Independent experiments were repeated at least three times, and the data were expressed as mean ± standard deviation for all triplicates within an individual experiment.

Magnetic Hyperthermia Studies

To investigate the magnetic hyperthermia efficiency for the colloidal magnetic NPs (S0–S4), 1 mg of the sample powder was dispersed in 1 mL distilled water (1 mg/mL) in accordance with the human body structure, then was sonicated for 2 min at a frequency of 1.15 MHz with acoustic energy and power of 500 J and 25 W, respectively. The hyperthermia conditions were provided by using an induction heating device (Easyheat 3542LI, 4 kW, Ambrell, Gloucestershire, UK)[42] with three varied currents of 75, 100, and 125 A, which respectively corresponded to frequencies of 318, 313, and 312 kHz. To reduce the temperature variation with the environmental condition, the Fe_3O_4 NPs dispersions were put inside a 2 mL glass vial surrounded by a polystyrene box.[29,43] The dispersed S0–S4 samples in a vial vertically were placed in the center of a short helical coil with 8-turned loops and 2.54, 2.92 and 5.10 cm in inner diameter, outer diameter, and length, respectively, and were cooled by water circulation to ensure constant temperature and impedance. Temperature changes over time (dT/dt) during the hyperthermia experiments were measured with a thermocouple connected to a data processing system to obtain T_H.

The generated magnetic field strengths (H) at different currents are determined using Equation 1:[42,44,45]

$$H = \frac{n \cdot i}{L} \quad (1)$$

Where n, i, and L represent the number of the coil turns, applied current (A), and inner coil diameter (m), respectively. The calculated values of AMF strength at 75, 100, and 125 A, were 23.6, 31.5, and 39.37 $kA.m^{-1}$, respectively. Heating efficiency of the Fe_3O_4 NPs samples are quantitatively estimated through SAR under the external AMF exposure for 3600 sec using Equation 2:[45]

$$SAR = \left(\frac{C_m.m_m}{m_{Fe}}\right)\left(\frac{dT}{dt}\right) \quad (2)$$

Where C_m is the specific heat capacity of the colloidal dispersion, including Fe_3O_4 and water medium with values of 0.65 $J.g^{-1}.K^{-1}$ and 4.18 $J.g^{-1}.K^{-1}$, respectively. The m_m was defined as the total mass of the colloidal dispersion comprised the medium and the Fe_3O_4 NPs sample (iron oxide and the extract as a stabilizer) at a concentration of 1 mg/mL, whereas $C_m\, m_m = (C_{medium} \times m_{medium}) + (C_{sample} \times m_{sample})$. Further, m_{Fe} shows the iron mass per unit of the Fe_3O_4 NPs sample (based on the Fe ratio),[44] and the dT/dt signifies the initial slope of the temperature profile.

Cell Lines and Culture Reagents

HCT116 colon cancer (ATCC CCL-247) and CCD112 colon normal (ATCC CRL-1541) cell lines were purchased from American Type Culture Collection (ATCC) and cultured according to ATCC's recommendation.[6,46] All cell lines were cultured in high-glucose Dulbecco's Modified Eagle's medium (DMEM) (#12800, Thermo Fisher Scientific) supplemented with 10% foetal bovine serum (FBS) (#10270-106, Thermo Fisher Scientific), and 1% penicillin/streptomycin (#15140-122, Thermo Fisher Scientific).

In vitro Cytotoxicity Assay

Cytotoxicity assays were conducted to verify the cellular killing effect of all the samples (S0–S5) by using CellTiter-Glo 2.0 Luminescent Cell Viability Assay (#G9241, Promega), according to the manufacturer's instruction with a slight modification.[6,46] Briefly, 5000 HCT116 and CCD112 cells per well (100 µL/well) were seeded onto a 96-well plate and incubated overnight (12–16 h) at 37°C in a 5% CO_2 and 95% humidified incubator. After that, 2-fold serially diluted samples at concentrations of 0, 15.62, 31.25, 62.53, 125, 250, 500 and 1000 (100 µL/well) were added into the wells and the plate was incubated for 72 h at 37°C in a 5% CO_2 humidified incubator.[16,47] Then, 100 µL of the reagent per well was added into the plate and incubated for 1 h at 37°C in 5% CO_2 incubator before the plate was read using a multimode microplate reader (Tecan). The dose–response graph was plotted by calculating percent cell viability using the equation below (Equation 3):

$$\%\ \text{Cell viability} = \frac{\text{OD of sample well (mean)}}{\text{OD of control well (mean)}} \times 100 \quad (3)$$

In addition, the inhibitory concentration, which caused 50% growth inhibition (IC_{50}) was determined, using an online calculator (https://www.aatbio.com/tools/ic50-calculator) as previously described.[16,46]

Independent experiments were repeated at least three times, and the data were expressed as mean ± standard deviation for all triplicates within an individual experiment. Data were analyzed using a Student's *t*-test. $p < 0.05$ was considered significant.

Results and Discussion

Reaction

Figure 1 indicates a schematic diagram of the possible chemical compounds in the crude extract of *G. mangostana* fruit peel, which served as a stabilizing agent and reacted with a mixture solution of Fe^{3+}/Fe^{2+} ions by using a facile co-precipitation method to produce Fe_3O_4 NPs. The formation of the green synthesized Fe_3O_4 NPs was observed through color change of the solution from purple to black. The observed response of the synthesized Fe_3O_4 NPs to an external magnet confirmed the magnetic properties of the NPs. The physiochemical properties of the green synthesized magnetic samples were studied, and the samples were evaluated by magnetic hyperthermia analysis and also their cytotoxicity assays were analyzed towards colon cancer cell line (HCT116) and normal cell line (CCD112).

X-Ray Diffraction (XRD) Analysis

Figure 2 shows the XRD spectra for the synthesized Fe_3O_4 NPs. The NPs present a similar pattern and diffraction peaks at 2θ = 30.44°, 35.82°, 43.47°, 53.92°, 57.45°, 63.01°, and 74.69°, which respectively are corresponding to (220), (311), (400), (422), (511), (440), and (533) crystal planes of the pure cubic spinel crystal structure phase of Fe_3O_4 based on the literature data (JCPDS file no: 00-003-0863).[6,16] Debye-Scherrer equation (Equation 4) was used to measure the crystallite size of the synthesized Fe_3O_4 NPs.[48]

$$D_{hkl} = \frac{K\lambda}{\beta_{hkl}\cos\theta} \quad (4)$$

Where hkl is the Miller indices of the lattice planes being examined, D_{hkl} is the size of crystallite in direction

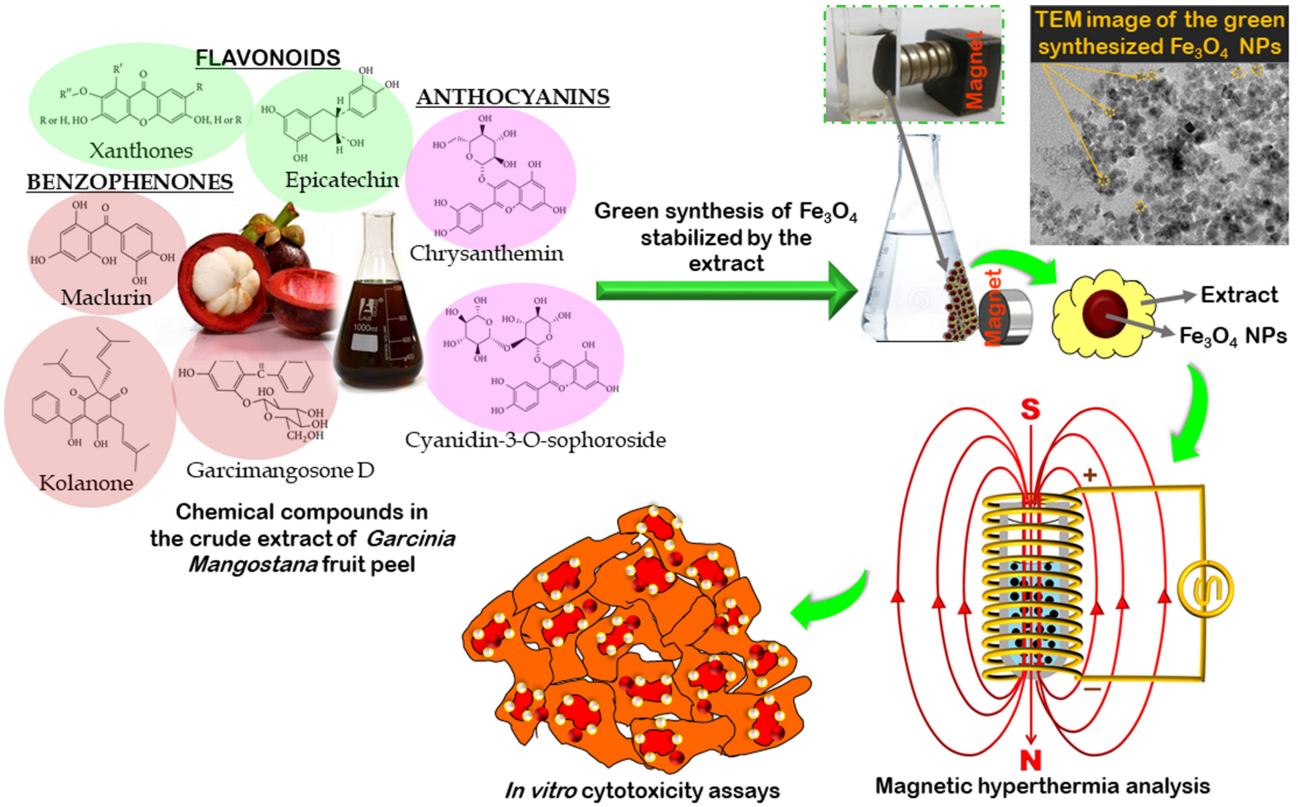

Figure 1 A schematic of the chemical compounds in the crude extract of *G. mangostana* fruit peel which served as a green stabilizer to synthesize Fe_3O_4 NPs for magnetic hyperthermia study and elimination of the colon cancer cells.

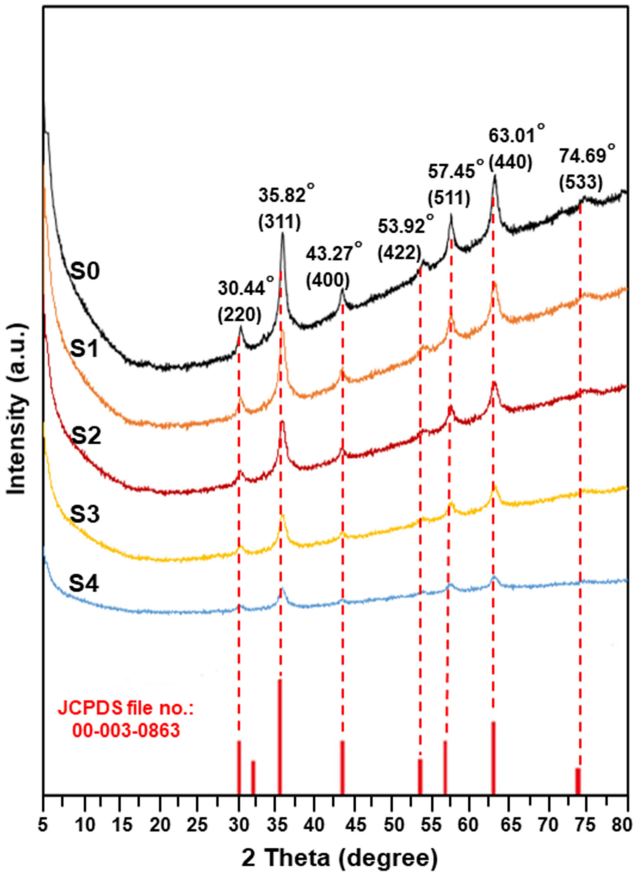

Figure 2 XRD spectra of the synthesized Fe_3O_4 NPs (S0–S4).

perpendicular to the lattice planes, K is the crystallite-shape factor with a Scherrer constant = 0.9 for an absence information of crystallite-shape, λ is a wavelength of X-rays = 0.154059 nm, β_{hkl} is a full width at half maximum (FWHM) of the XRD diffraction peak in radians in 2θ scale, and θ is the half diffraction angle of the peak.[49] By using the equation above, crystallite size of the strongest reflection at 35.82° (311) peak for S0, S1, S2, S3, and S4 samples was 12.84 nm, 12.03 nm, 11.52 nm, 9.34 nm, and 7.81 nm, respectively. From the XRD patterns of all the samples, purity of the crystalline phase was acceptable due to low impurity peaks. Therefore, the above results could indicate the successful use of the extract as a green stabilizer in the synthesis of Fe_3O_4 NPs (magnetite phase).

Transmission Electron Microscopy (TEM)

Figure 3A–D illustrate TEM image, particle size distribution, selected area electron diffraction (SAED) pattern, and electron diffraction pattern of the S2 sample, respectively. As seen in Figure 3A, most of the particles were nearly spherical with potentially good dispersity and minor agglomeration. The presence of the agglomeration could be due to the van der Waals forces for binding particles together and also shear forces that can be applied on the nanoscale.[50] In addition, the presence of the hydroxyl groups in the peel extract could possibly led to the agglomeration. A histogram of the NP size distribution was plotted with 220 counts as shown in Figure 3B. The size distribution was in a range of 6 to 20 nm with a mean size of 13.42±1.58 nm, and a standard deviation of 2.74±0.16 nm. Based on the SAED pattern in Figure 3C, diffraction rings of the Fe_3O_4 phase were indexed as (311), (220), (400), (422), (511), (440) and (533), which was in good agreement with the XRD results.[6] Figure 3D shows electron diffraction pattern of S2, indicating a regular and uniform crystallinity with lattice spacing on TEM image around 0.28 nm. Therefore, TEM study displayed that the biosynthesized Fe_3O_4 NPs possessed nearly spherical shapes with good crystallinity.

Field Emission Scanning Electron Microscopy (FESEM) and Energy Dispersive X-Ray Spectroscopy (EDS)

Figure 4A and B demonstrate FESEM images and EDS of S0–S5, respectively. As seen in the images, the nano-sized particles were nearly spherical. In addition, the peel extract potentially rolled as a protective agent to cover the surface area of the Fe_3O_4 NPs. Thus, increasing the coating ratio around the NPs was in line with the enhancement of the extract concentration. However, this coating layer may not be seen for S0 as a naked Fe_3O_4 NPs. Irregular shapes were detected because of the agglomeration process possibly related to the strong inter-particles and Van der Waals forces, high surface area to volume ratio, and magnetic attraction among the Fe_3O_4 NPs.[6,51] The S5 sample illustrated the image of the peel extract with an unorganized structure. Figure 4B indicates EDS spectra of the samples. The extract powder (S5) presented 64.70 wt.% and 35.80 wt.% of carbon and oxygen, respectively. These components were potentially deposited in the green synthesized Fe_3O_4 NPs. Thus, the samples containing higher concentration of the peel extract possessed higher proportion of carbon and oxygen. In this manner, the ratio of carbon was higher in S4 than S1, showing the successful use of the extract as a stabilizer in the green synthesis of Fe_3O_4 NPs. Therefore, EDS spectrum of the Fe_3O_4 samples exhibited

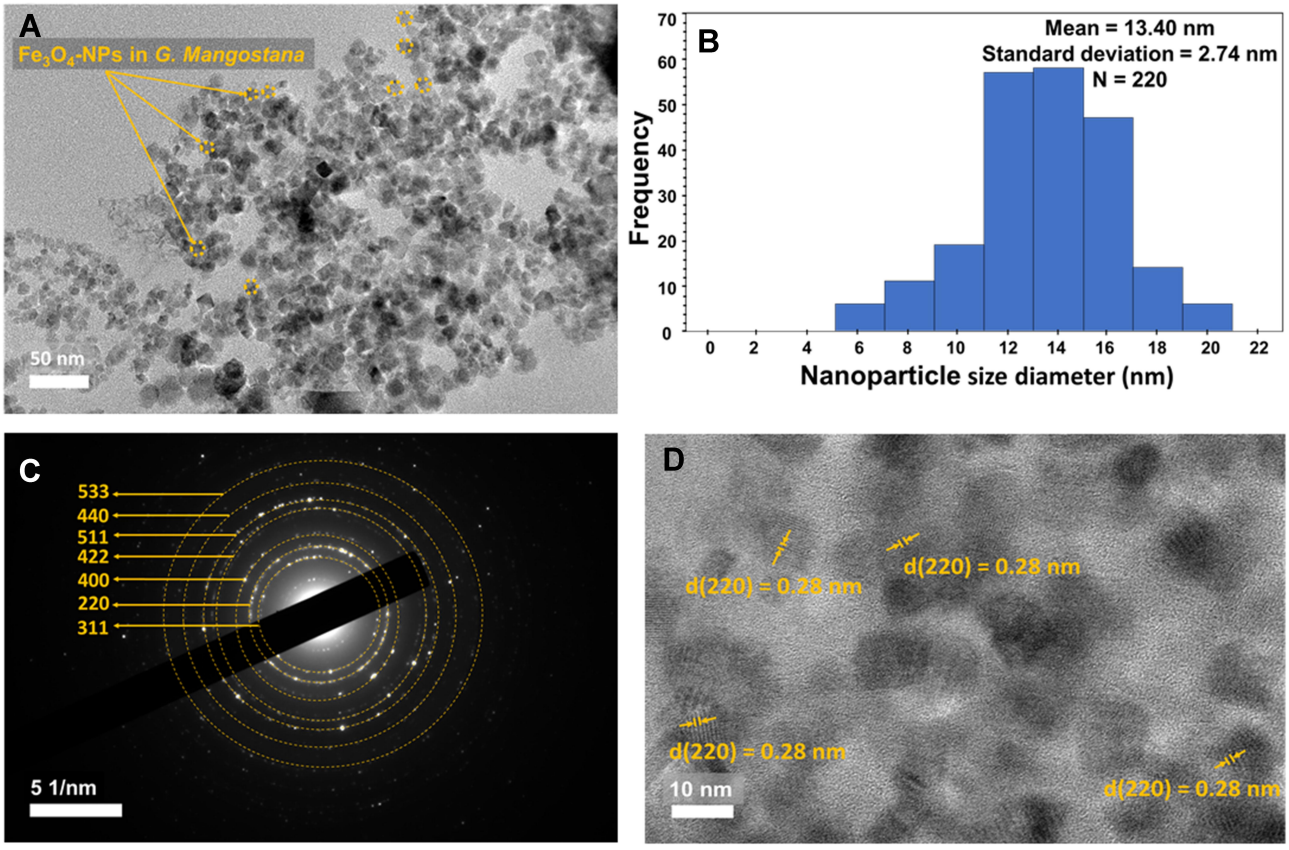

Figure 3 (**A**) TEM image, (**B**) histogram of the Fe_3O_4 NPs distribution, (**C**) SAED pattern, and (**D**) electron diffraction pattern of the synthesized Fe_3O_4 NPs of S2.

good purity of the compounds, owing to the presence of iron, carbon, and oxygen elements.

Vibrating-Sample Magnetometer (VSM)

The VSM study of the synthesized Fe_3O_4 samples is illustrated in Figure 5A and B. The saturation magnetization of S0–S4 was found to be 73.15, 69.42, 64.35, 59.50, and 49.80 emu/g, respectively, at room temperature. The samples with the higher extract ratio showed lower magnetic properties, indicating the contribution of the extract stabilizer for the biosynthesis of Fe_3O_4 NPs. When the magnetic field was removed, an increase in the applied field rose the magnetic moment/mass. Hysteresis loops occurred when the external magnetic field was applied to the NPs,[52] and magnetization decreased from a plateau value to zero. The increase of the extract ratio decreased and increased the saturation magnetization and the coercivity of the samples, respectively. Of this, among the Fe_3O_4 samples, S0 as a bare magnetic NPs indicated the lowest coercivity of 10.80 Oe and the highest saturation magnetization of 73.15 emu/g. However, S4 containing the highest extract ratio (10 wt.%) showed the highest coercivity (87.21 Oe) and the lowest saturation magnetization (49.80 emu/g). This is due to the non-magnetic nature of the extract as coated the magnetic NPs. It can be understood from the VSM results, the green synthesized Fe_3O_4 NPs could be conveyed by an external magnetic field and potentially directed to a specific target inside the body for biomedical applications, although future studies would need to focus on.

Fourier-Transform Infrared Spectroscopy (FTIR)

Figure 6 shows FTIR spectra of S0–S5. The samples with higher concentration of the extract stabilizer displayed transmittance peaks closer to the crude extract alone in a similar wavenumber range. The intensity of C=O stretching vibration and C-O stretch increased due to the presence of the carbonyl group in the anthocyanin structure and alcohol group, respectively.[53] In the green synthesized Fe_3O_4 NPs samples (S1-S4), a broad band between 1621 cm^{-1} and 1649 cm^{-1} could be due to C=O stretching

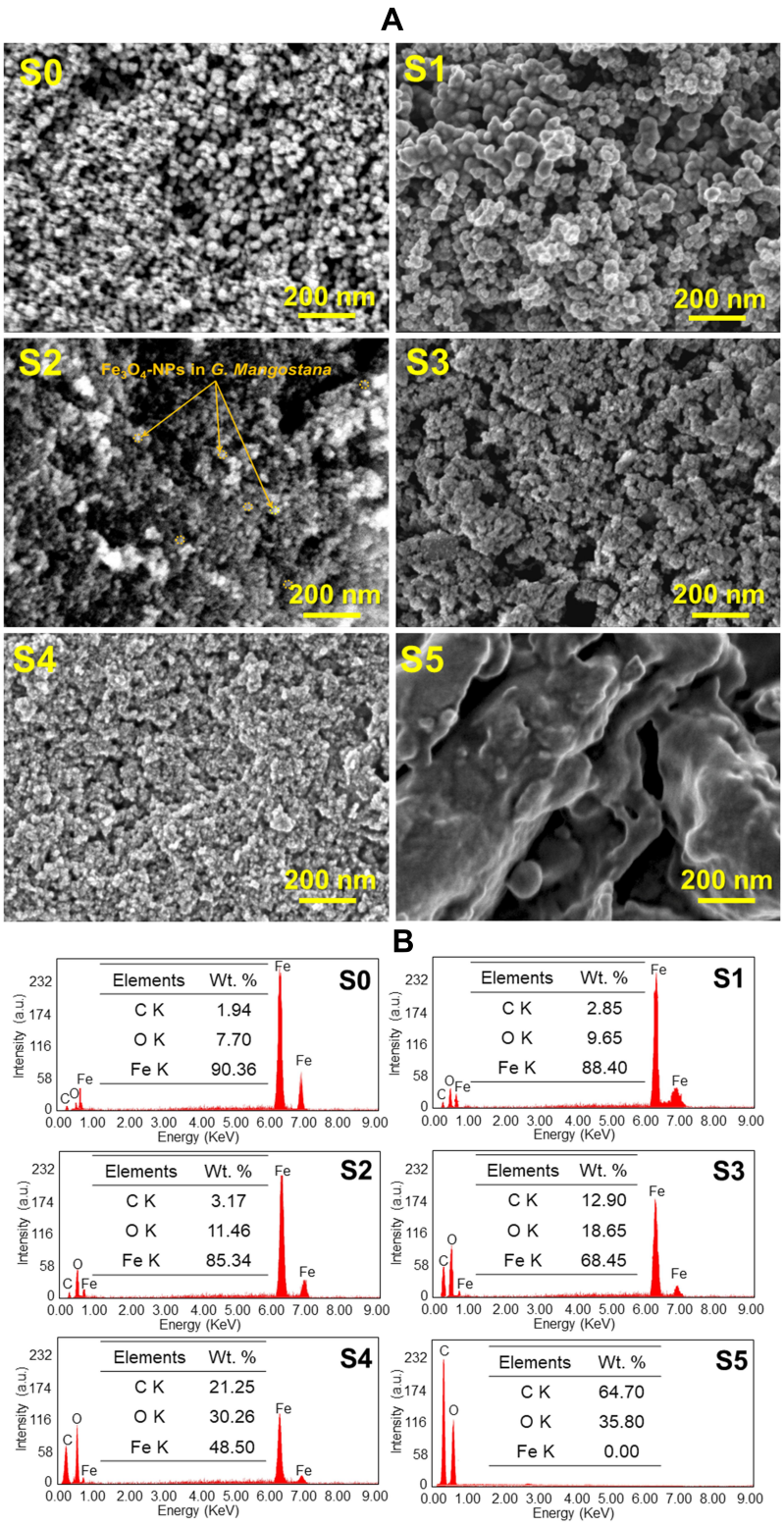

Figure 4 (**A**) FESEM image (scale bar = 200 nm ——) and (**B**) EDS spectra of the synthesized Fe_3O_4 NPs (S0–S4) and the crude extract of *G. mangostana* fruit peel (S5).

vibration.[6] Furthermore, the peaks in a range from 3442 cm^{-1} to 3596 cm^{-1} were assigned to the hydroxyl group, representing the O-H stretching vibration, which was higher for the Fe_3O_4 NPs samples with the higher extract ratio. The functional groups of O-H, C=O, and C-O could possibly indicate the presence of gartanin

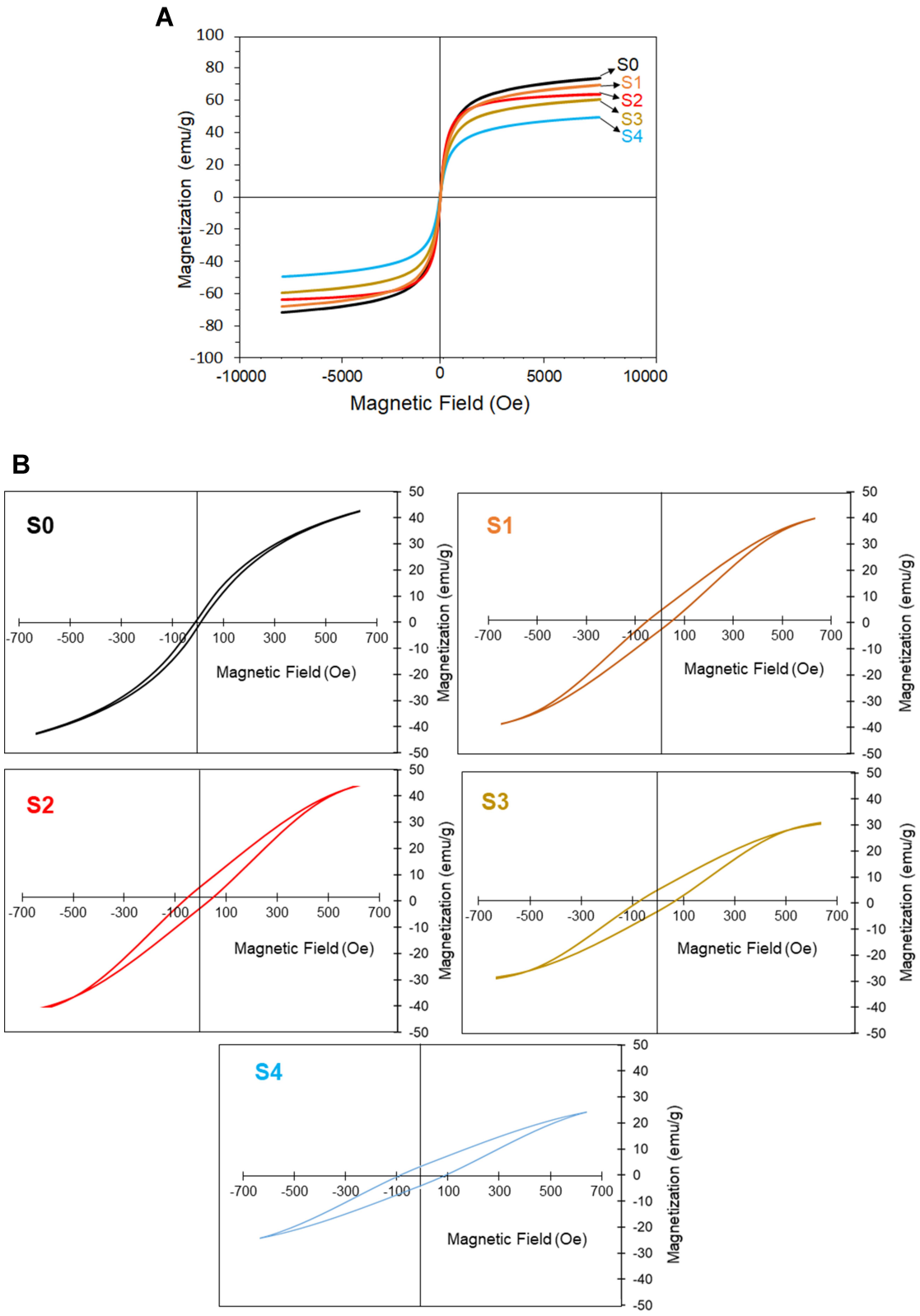

Figure 5 (**A**) Saturation magnetization and (**B**) coercivity of the synthesized Fe_3O_4 NPs (S0–S4).

compound in the samples. Gartanin is a chemical compound in xanthone isolated from *G. mangostana* fruit peel.[54] In all spectra of the synthesized Fe_3O_4 NPs, peaks appeared at a range from 636 cm^{-1} to 721 cm^{-1}, showing characteristic of metal-oxygen band, which was the Fe-O stretching vibration of Fe_3O_4 NPs.[55] These

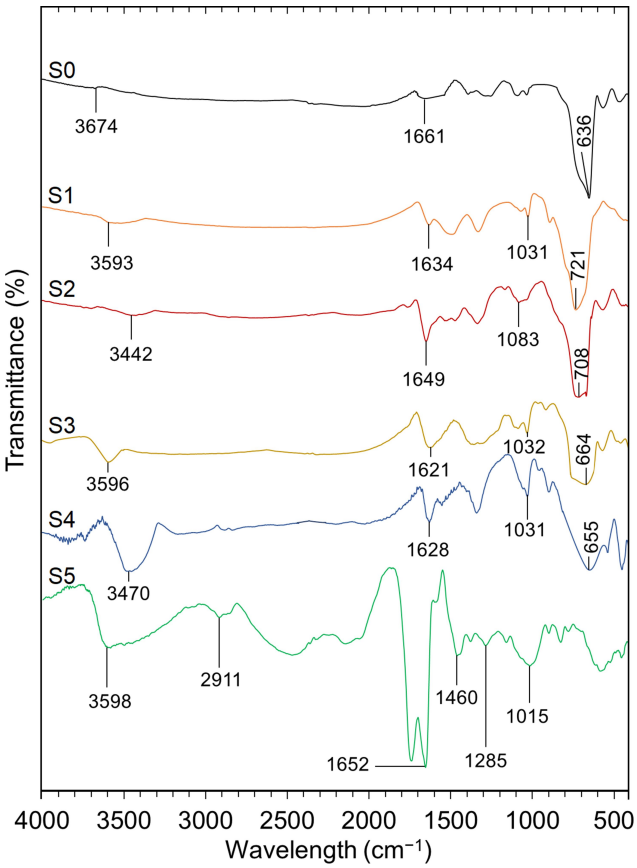

Figure 6 FTIR spectra of the synthesized Fe_3O_4 NPs (S0–S4) and the crude extract of *G. mangostana* (S5).

stretching vibration bands could be linked to the metal in the tetrahedral and octahedral site.[56] Based on FTIR analysis of Fe_3O_4 NPs stabilized with *Lagenaria siceraria* extract, the stretching vibration at 3354 cm^{-1}, 1701.55 cm^{-1}, and 624 cm^{-1} represented the presence of O-H bond stretching, C=O stretching, and Fe-O stretching, respectively.[6] From the FTIR spectrum of S5, a peak at 3598 cm^{-1} was assigned to the presence of O-H stretch and H-bonding and a peak at 2911 cm^{-1} indicated the C-H stretching vibration band.[53] The characteristic of the carbonyl group is the C=O stretching vibration at 1652 cm^{-1}, whereas, the presence of the aromatic group was indicated by the band at 1460 cm^{-1}. The peaks between 1300 cm^{-1} to 1000 cm^{-1} were attributed to the functional group of C-O as it potentially related to the alcohols, ethers, ester, carboxylic acids, and amides in the crude extract of *G. mangostana* fruit peel.[53] Compared to other green synthesized Fe_3O_4 NPs, the extract showed the highest impact on the S4 sample, which contained the highest extract ratio (10 wt.%). In this manner, the O-H stretching peak of the extract's spectrum shifted from 3598 cm^{-1} to 3470 cm^{-1} after the biosynthesis of Fe_3O_4 NPs. Meanwhile, the peak for the C=O and C-O stretching vibration of S5, respectively, shifted from 1652 cm^{-1} to 1628 cm^{-1} and from 1015 cm^{-1} to 1031 cm^{-1} after capping with Fe_3O_4 NPs in the S4 sample. Thus, the FTIR results could indicate that the extract successfully served as both stabilizing and capping agents during the green synthesis process of the Fe_3O_4 NPs.

Dynamic Light Scattering (DLS) Analysis and Impact of Storage Time on Fe_3O_4 Nanofluids

Table 1 depicts DLS results with values of zeta potential, hydrodynamic size, and polydispersity index of the samples, respectively. Adding the extract stabilizer increased the zeta potential value and also the hydrodynamic size. Among the synthesized magnetite samples, S0 as a bare Fe_3O_4 NPs sample had the lowest hydrodynamic size and the zeta potential value of 95.93±2.2 nm and −20.72±1.7 mV, respectively. Although, S4 with the highest stabilizer concentration (10 wt.%) showed the highest hydrodynamic size and zeta potential value of 176.15±1.46 nm and −34.92±1.26 mV, respectively. This may exhibit that coating the NPs with the plant extract provided a repulsive force between the NPs.[57] Compared to the TEM size, the DLS size was larger for S2. This can be explained that DLS indicates the combination of particle size and surrounding diffuse layer of the particle; however, TEM analysis is attributed to the particle size alone. In the aqueous media, the presence of the particle−particle interactions affected hydrophobic attraction energy between Fe_3O_4 NPs to attract each other, albeit, hydrophilic extract potentially governed hydrophilicity of the NPs to improve their thermodynamic stabilities.[58] The extract may also act as a tailoring agent to improve the surface features of the synthesized Fe_3O_4 NPs in the aqueous media. As value of zeta potential increased, polydispersity index decreased, showing that zeta potential was inversely attributed to polydispersity index. All the samples displayed the polydispersity index values below 0.7. This indicates that the extract of *G. mangostana* fruit peel as a new stabilizer potentially caused the nucleation of the Fe_3O_4 with a narrow dispersity.[6] In a different study, Sathishkumar et al[57] synthesized Fe_3O_4 NPs using a stabilizer of *Couroupita guianensis* Aubl. fruit extract, that the zeta potential of the fabricated NPs was found to be −26 mV.

Table 1 Zeta Potential, Hydrodynamic Particle Size, and Polydispersity Index of the Synthesized Sample Suspensions During Four Weeks of Storage

	As-Prepared	After 1 Week of Storage	After 2 Weeks of Storage	After 3 Weeks of Storage	After 4 Weeks of Storage
Sample	**Zeta potential (mV)**				
S0	−20.72±1.7	−16.96±1.1	−15.26±2.2	−14.58±1.6	−12.00±1.6
S1	−25.61±1.8	−24.32±0.5	−23.77±1.3	−22.24±1.4	−20.22±1.9
S2	−28.64±1.3	−27.44±1.0	−26.92±1.2	−25.14±0.2	−22.71±1.5
S3	−29.58±1.1	−27.87±1.4	−25.45±1.8	−25.17±1.3	−24.36±1.4
S4	−34.92±1.2	−34.25±0.9	−33.14±1.1	−31.83±2.2	−30.15±2.7
S5	−15.66±1.2	−11.54±2.0	−8.23±2.3	−7.65±1.5	−6.82±0.5
Hydrodynamic particle size (nm)					
S0	95.93±2.2	97.23±1.6	109.98±1.3	125.00±1.2	134.00±2.6
S1	107.90±0.2	110.09±1.3	115.27±0.5	121.20±1.1	128.20±2.1
S2	120.34±1.7	125.47±1.0	127.54±1.2	130.90±1.0	134.84±1.5
S3	145.82±1.0	150.63±1.4	150.81±1.8	158.28±1.4	165.61±2.1
S4	176.15±1.4	180.35±0.9	184.00±1.1	190.44±1.8	198.27±2.0
Polydispersity index					
S0	0.31±0.03	0.40±0.06	0.42±0.03	0.45±0.02	0.50±0.06
S1	0.29±0.02	0.35±0.04	0.38±0.05	0.40±0.01	0.41±0.07
S2	0.27±0.02	0.31±0.06	0.33±0.02	0.35±0.04	0.39±0.09
S3	0.25±0.04	0.29±0.09	0.33±0.06	0.34±0.04	0.35±0.02
S4	0.23±0.01	0.25±0.03	0.28±0.04	0.30±0.08	0.32±0.04

As provided in Table1, the zeta potential values of S0–S4 after the storage of 1, 2, 3, and 4 weeks were slightly and gradually decreased. This can indicate the low particle agglomeration and aggregation are in the line with time, which is similar to different reports.[41,59] The zeta potential values exhibited that the Fe_3O_4 NPs suspensions with the higher extract ratio could present better colloidal stability than those NPs with the lower extract ratio after 4 weeks of storage. Particle size of the magnetic nanofluid samples at different storage time was obtained from DLS measurement (Table 1). Figure 7A and B show the hydrodynamic size distributions of S0–S4 as prepared and after 4 weeks of storage, respectively. An increase in the average particle size after the prolonged storage could be related to a minor agglomeration in the Fe_3O_4 NPs. Albeit, there was no major agglomeration visually noticed on the sample suspension even after 4 weeks of storage. In addition, the polydispersity index values were almost unchanged with the values below 0.7 even after 4 weeks of storage. Therefore, the Fe_3O_4 NPs suspensions displayed good stability during 4 weeks of storage.

Magnetic Hyperthermia Study

The hyperthermia performance of the Fe_3O_4 NPs samples was assessed through measuring their temperature rise under the exposure of different AMF strengths to determine the minimal AMF strength. Further, the T_H maintained within the secure hyperthermia range in order to prevent unpredictable disorders and subsequently perform a successful MHT. The thermal profiles of the nanofluid samples containing 1 mg/mL of Fe_3O_4 NPs under the exposure of varied AMF strengths of 23.60, 31.50, and 39.37 $kA.m^{-1}$ over 3600 sec are illustrated in Figure 8. All the graphs illustrate almost a similar thermal behavior throughout the treatment time under different AMF exposure. Clearly shown that the temperature increased significantly until 360 sec (Phase 1), followed by a moderate temperature rise until heating intervals of approximately 1800 sec (phase 2). Then, the temperature raised negligibly in the aqueous medium (phase 3). The highest effect of the AMF strength was observed in phase 1, where the slope of the temperature rise (dT/dt) at this stage which was significantly higher than the other phases. Hence, the slope of the phase 1 for all of the thermal profiles was considered for the SAR value measurements. The SAR

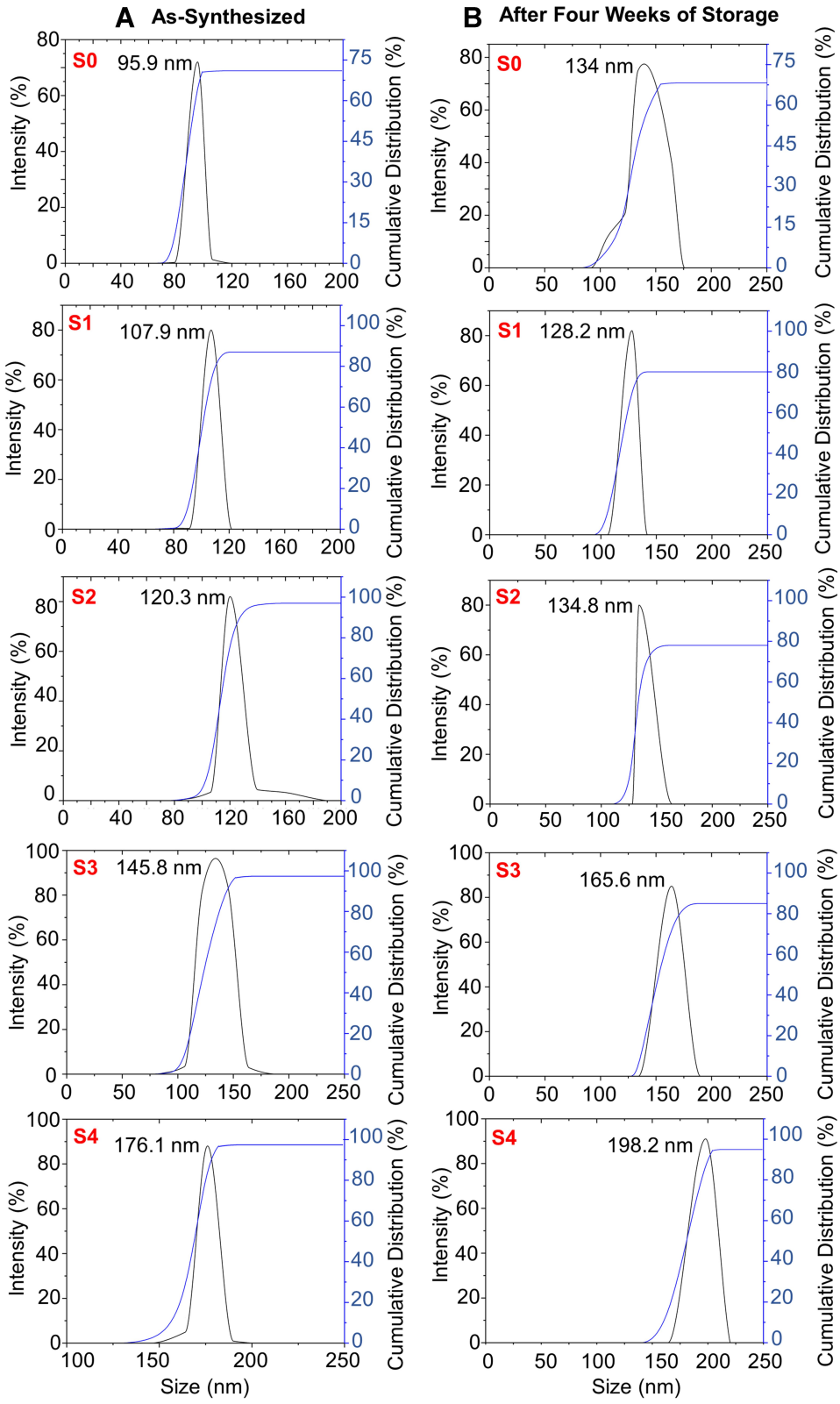

Figure 7 Hydrodynamic size distributions of the nanofluid samples containing Fe_3O_4 NPs (**A**) as-synthesized and (**B**) after four weeks of storage.

values of the nanofluid samples exposed to different AMF strengths are provided in Table 2. The SAR values increased considerably with increasing AMF strengths from 23.60 $kA.m^{-1}$ to 39.37 $kA.m^{-1}$ due to the heating loss mechanisms,[60] which is also in line with previous research reports such as bare superparamagnetic Fe_3O_4[44]

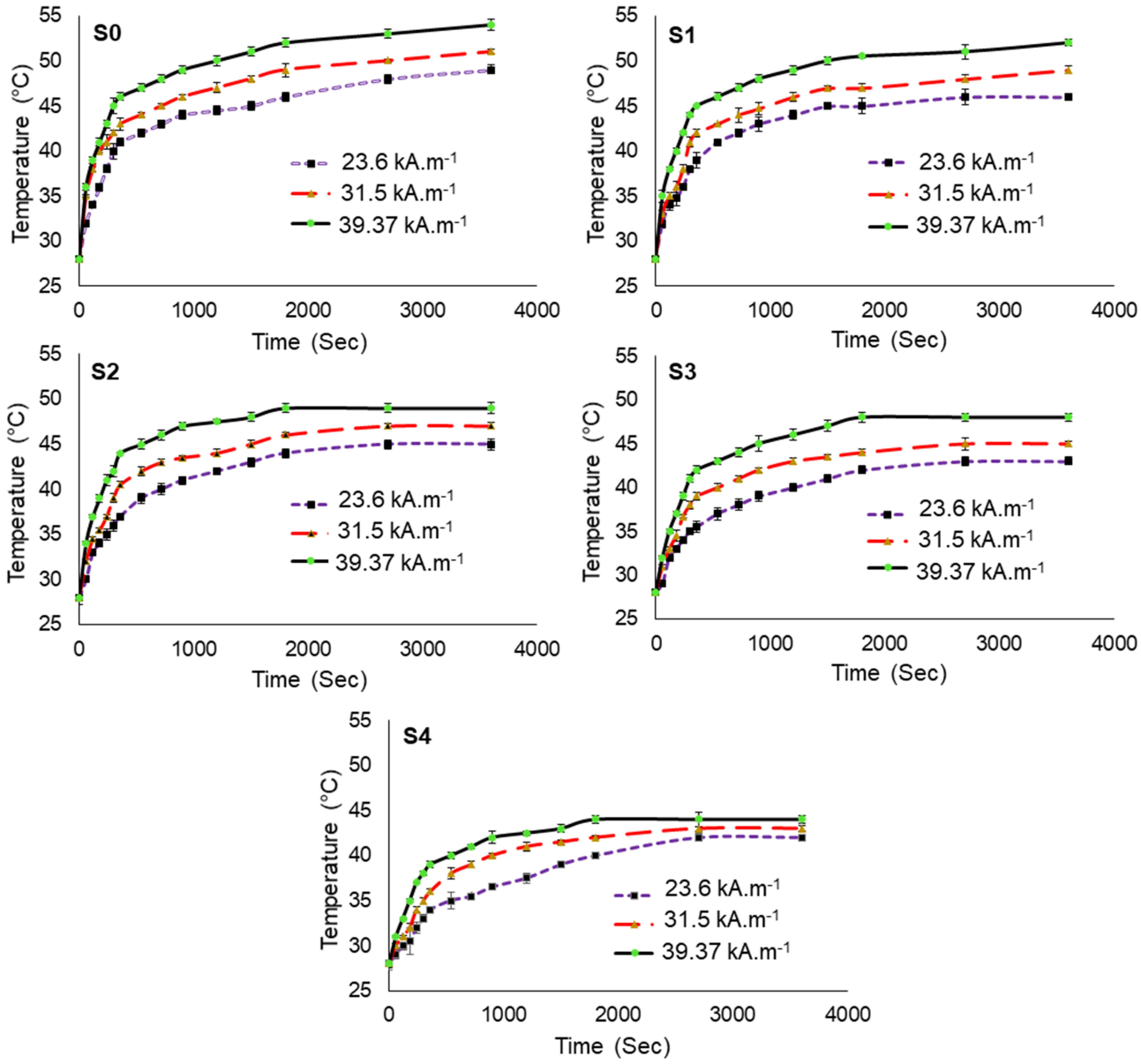

Figure 8 The temperature profiles of the nanofluid samples containing the synthesized Fe_3O_4 NPs of S0–S4, which were obtained after exposure to the varied AMF strengths of 23.60 $kA.m^{-1}$, 31.50 $kA.m^{-1}$, and 39.37 $kA.m^{-1}$.

and polycaprolactone-coated Fe_3O_4[45] and γ-Fe_2O_3.[42] The SAR values reduced remarkably with increasing the extract concentrations from 0 to 10 wt.%, which might be ascribed to the non-magnetic nature, which acted as a heating barrier for the Fe_3O_4 NPs. Thereby, the highest and the lowest SAR values were respectively obtained for S0 and S4 at each AMF strength. Nevertheless, S1 with the lowest extract concentration could render significant SAR value as compared to other extracted counterparts with values of 165.74±0.5 $W.g^{-1}$, 212.06±0.4 $W.g^{-1}$, and 246.86±0.2 $W.g^{-1}$ at 23.6 $kA.m^{-1}$, 31.5 $kA.m^{-1}$, and 39.37 $kA.m^{-1}$, respectively.

Although the S0 sample could show the highest SAR values over the range of AMF strengths, this sample was incapable of maintaining T_H at the secure hyperthermia range (42–47°C) even at the minimal applied AMF strength of 23.6 $kA.m^{-1}$. However, the extract could potentially control the medium temperature of the nanofluid under the hyperthermia condition to produce sufficient thermal energy within the secure hyperthermia range.[56] The data provided in Table 2 clearly implies that the S4 sample with the highest extract concentration (10 wt.%) could retain a medium temperature rise within the secure hyperthermia range which is appropriate for

Table 2 The Achieved Hyperthermia Properties of the Nanofluid Samples Containing Fe_3O_4 NPs and Varied Extract Concentrations Exposed to Different AMF Strengths Over 360 Sec

Sample	Frequency (kHz)	Current (A)	AMF Strength ($kA.m^{-1}$)	T_H (°C)	SAR ($W.g^{-1}$)
S0	318	75	23.6	49±0.2	188.67±0.5
	313	100	31.5	51±0.2	218.64±0.3
	312	125	39.37	54±0.6	260.96±0.4
S1	318	75	23.6	46±0.3	165.74±0.5
	313	100	31.5	49±0.4	212.06±0.4
	312	125	39.37	52±0.3	246.86±0.2
S2	318	75	23.6	45±0.4	144.59±0.5
	313	100	31.5	47±0.3	195.72±0.2
	312	125	39.37	49±0.6	239.80±0.4
S3	318	75	23.6	43±0.5	128.72±0.3
	313	100	31.5	45±0.3	178.79±0.2
	312	125	39.37	48±0.4	225.70±0.3
S4	318	75	23.6	42±0.2	98.74±0.6
	313	100	31.5	43±0.2	130.48±0.3
	312	125	39.37	44±0.4	179.85±0.1

prospective hyperthermia treatment. The S4 solution indicated temperature rise (with the SAR values) of 42±0.2°C (98.74±0.6 $W.g^{-1}$), 43±0.2°C (130.48±0.3 $W.g^{-1}$) and 44±0.4°C (179.85±0.1 $W.g^{-1}$) at AMF strengths of 23.6 $kA.m^{-1}$, 31.5 $kA.m^{-1}$, and 39.37 $kA.m^{-1}$, respectively. The extract of *G. mangostana* peel as a novel stabilizer could trigger a positive effect on Fe_3O_4 NPs preparation to perform a successful MHT. Therefore, according to the obtained magnetic hyperthermia results from Table 2, the synthesized Fe_3O_4 NPs stabilized with the extract could be considered as a promising candidate for hyperthermia therapy of cancer.

In vitro Cytotoxicity Assay

Figure 9A and B demonstrate the cytotoxic effects of S0–S5 against colon cancer (HCT116) and normal cell lines (CCD112) after 72 h of treatment, respectively. Dose-dependent killing effect was seen in all the tested samples in both cell lines. Table 3 indicates the IC_{50} of S0–S5 against the colon cancer and normal cell lines. The crude extract *of G. mangostana* fruit peel showed higher anticancer activity compared to the extracts of different plants such as *Punica granatum* fruit peel,[6] *Juglans regia* green husk,[16] and *seaweed (Kappaphycus alvarezii)*.[61] This could be due to the presence of xanthone and α-mangostin in the crude extract of *G. mangostana* peel.[62] Among all the magnetic samples, S4 with the highest extract concentration (10 wt.%) showed the highest killing effect against the cancer cells with the lowest IC_{50} (99.8 µg/mL). The IC_{50} of S4 in the normal cells was found to be 140.80 µg/mL, which was slightly higher than that of the cancer cells. Figure 10 summarizes the toxicity of S4 on HCT116 cancer and CCD112 normal cell lines. At 125 µg/mL and 250 µg/mL, S4 killed 52±0.54% and 63±1.68% of the cancer cells, respectively. At 500 µg/mL and 1000 µg/mL, S4 caused respectively, 72±1.15% and 80±0.61% killing effects against the cancer cells; however, it displayed 63±2.17% and 68±1.05% elimination of the normal cells, respectively. The anticancer activity of the magnetic samples possibly could be due to release of iron ions from the Fe_3O_4 NPs following its breakdown and the subsequent Fe reutilization process by cells for Fe metabolism, which could be one of the cancer cell killing mechanisms.[63] It is worth mentioning that the extract as a stabilizer and capping agent possibly tailored assemblies of Fe_3O_4 NPs with a temperature-responsive structure, and self-heating capacity to destroy the cancer cells. The nucleation of the NPs in the presence of the extract was translated into an efficient bonding between the phenolic compounds of the extract into/onto the NPs to strongly avoid deep oxidation, possibly suitable for various biomedical applications.[13,15] As previously reported,[64] normal cells could decrease their heat-sensitivity five or six times than that of the growing situation at the conflux, but the cancer cells were unable. In this manner, cancer cells might indicate higher temperature (above 37°C) compared to normal cells (below 37°C).

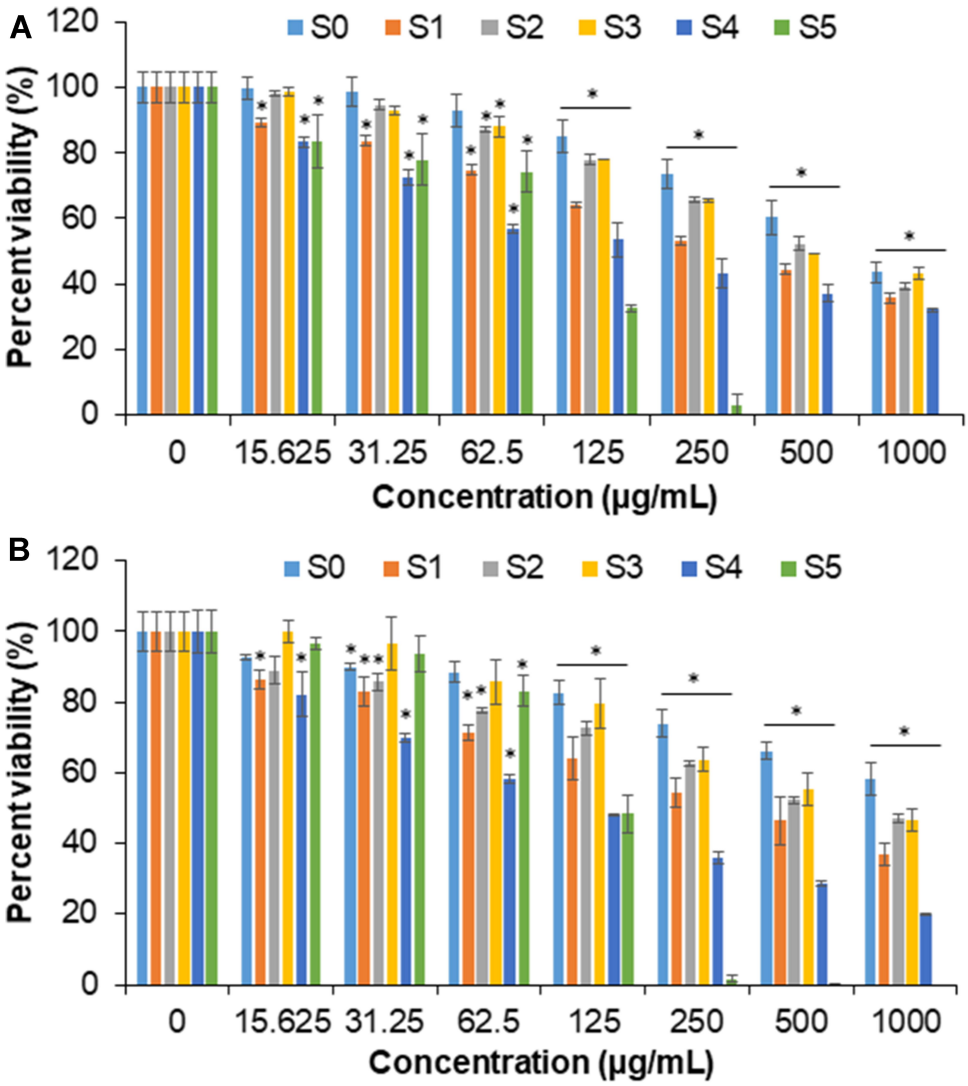

Figure 9 Relative viability of (**A**) CCD112 colon normal cell line and (**B**) HCT116 colon cancer cell line treated with the synthesized Fe_3O_4 NPs (S0–S4) and the crude extract of *G. mangostana* (S5). Data are expressed as mean ± standard deviation for triplicates within an individual experiment. Statistical significance was performed using a Student's *t*-test (*$p < 0.05$).

This slightly increased temperature of the cancer cells might trigger higher release of the phenolic compounds against the cancer cells. To our best understanding from these in vitro results, certain concentrations of the biosynthesized Fe_3O_4 NPs effectively eliminated the colon cancer cells; however, further improvements such as surface modifications and/or polymer coating on the NPs may decrease the toxicity of the *G. mangostana*/Fe_3O_4 samples on the normal cells.

Table 3 Inhibitory Concentration (IC_{50}) of S0–S5 on HCT116 and CCD112 Cell Lines

Sample	IC_{50} of HCT116 (µg/mL)	IC_{50} of CCD112 (µg/mL)
S0	>1000	750.1
S1	347.6	315.3
S2	698.9	542.6
S3	716.5	539.1
S4	99.8	140.8
S5	133	93.5

Conclusion

In this work, the green synthesis of Fe_3O_4 NPs was conducted by using a novel stabilizer of the crude extract of *G. mangostana* fruit peel at various concentrations (1, 2, 5, and 10 wt.%). TEM analysis of the magnetic sample containing 2 wt.% of the extract showed the spherical NPs with an average size of 13.42±1.58 nm and its SAED pattern was related to the Fe_3O_4 magnetite phase, which was in well agreement with the XRD data. Based on the

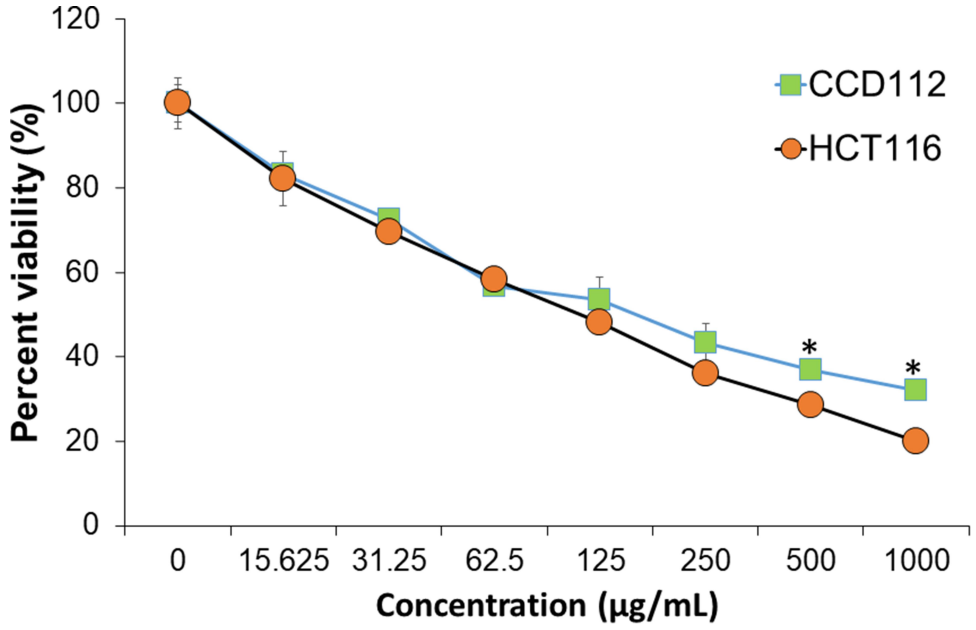

Figure 10 Relative viability of CCD112 colon normal cell lines and HCT116 colon cancer cell lines treated with Fe_3O_4 NPs of S4 containing 10 wt.% of *G. mangostana* peel extract.

FESEM images, the green synthesized NPs were surrounded by the extract. The saturation magnetization values of the samples with the lowest and highest extract concentration were 49.80 emu/g and 69.42 emu/g, respectively. The FTIR data indicated that the green synthesized Fe_3O_4 NPs contained the spectroscopy peaks related to the iron and the extract with xanthone, carboxylic, alcohol, and aromatic groups. The Fe_3O_4 nanofluids containing the highest ratio of the extract stabilizer indicated an improved particle charge of −34.92±1.26 mV and hydrodynamic size of 176.15±1.46 nm. Furthermore, the DLS analysis exhibited that the Fe_3O_4 nanofluids showed the colloidal stability even after 4 weeks of storage. The Fe_3O_4 nanofluids can be potentially used in hyperthermia therapy, since they mostly caused the T_H increase at the secure hyperthermia range (42–47°C) and the acceptable SAR values with the thermosensitive performances under exposure to AMF. Cytotoxicity assays of the samples were evaluated against CCD112 normal and HCT116 colon cancer cells. Particularly, the Fe_3O_4 NPs containing 10 wt.% of the extract showed a lower IC_{50} value (99.80 µg/mL) in HCT116 than in CCD112 (140.80 µg/mL). Consequently, this study indicated that the extract of *G. mangostana* fruit peel is a low-cost stabilizing and capping agent to improve the colloidal stability and physiochemical properties of the Fe_3O_4 NPs for potential hyperthermia therapy and anticancer treatments. Further investigations can lead to enhance the selectivity of the samples towards the cancer cells with the minimal toxicity on the normal cells. It can be considered to load an anticancer drug onto the green synthesized Fe_3O_4 NPs for the future study.

Acknowledgments

This research was funded by Takasago Thermal Engineering Co. Ltd. grant (#4B422) from the research management center (RMC) of Universiti Teknologi Malaysia (UTM) and Malaysia-Japan International Institute of Technology (MJIIT). Special thanks to School of Medical and Life Sciences, Sunway University Malaysia for the cell culture and laboratory facilities for the in vitro studies. This work was also supported by the UHK project VT2019-2021.

Disclosure

The authors declare no conflicts of interest for this work.

References

1. Yew YP, Shameli K, Miyake M, et al. Green biosynthesis of superparamagnetic magnetite Fe_3O_4 nanoparticles and biomedical applications in targeted anticancer drug delivery system: a review. *Arab J Chem*. 2020;13(1):2287–2308. doi:10.1016/j.arabjc.2018.04.013
2. Wu W, Wu Z, Yu T, Jiang C, Kim W-S. Recent progress on magnetic iron oxide nanoparticles: synthesis, surface functional strategies and biomedical applications. *Sci Technol Adv Mater*. 2015;16(2):023501. doi:10.1088/1468-6996/16/2/023501

3. Abdullah NH, Shameli K, Abdullah EC, Abdullah LC. Solid matrices for fabrication of magnetic iron oxide nanocomposites: synthesis, properties, and application for the adsorption of heavy metal ions and dyes. *Compos B Eng*. 2019;162:538–568. doi:10.1016/j.compositesb.2018.12.075
4. Arteaga-Díaz SJ, Meramo-Hurtado SI, León-Pulido J, Zuorro A, González-Delgado AD. Environmental assessment of large scale production of magnetite (Fe_3O_4) nanoparticles via coprecipitation. *Appl Sci*. 2019;9(8):1682. doi:10.3390/app9081682
5. Medina-Llamas M, Taylor CM, Ji J, Wenk J, Mattia D. Continuous production of metal oxide nanoparticles via membrane emulsification–precipitation. *Ind Eng Chem Res*. 2020;59(19):9085–9094. doi:10.1021/acs.iecr.0c00603
6. Yusefi M, Shameli K, Ali RR, Pang S-W, Teow S-Y. Evaluating anticancer activity of plant-mediated synthesized iron oxide nanoparticles using *Punica granatum* fruit peel extract. *J Mol Struct*. 2020;1204:127539. doi:10.1016/j.molstruc.2019.127539
7. Arias LS, Pessan JP, Vieira APM, Lima TMTD, Delbem ACB, Monteiro DR. Iron oxide nanoparticles for biomedical applications: a perspective on synthesis, drugs, antimicrobial activity, and toxicity. *Antibiotics*. 2018;7(2):46. doi:10.3390/antibiotics7020046
8. Jahangirian H, Azizi S, Rafiee-Moghaddam R, Baratvand B, Webster TJ. Status of plant protein-based green scaffolds for regenerative medicine applications. *Biomolecules*. 2019;9(10):619. doi:10.3390/biom9100619
9. Khandanlou R, Ahmad MB, Masoumi HRF, Shameli K, Basri M, Kalantari K. Rapid adsorption of copper (II) and lead (II) by rice straw/Fe_3O_4 nanocomposite: optimization, equilibrium isotherms, and adsorption kinetics study. *PLoS One*. 2015;10(3):e0120264. doi:10.1371/journal.pone.0120264
10. Magro M, Vianello F. Bare iron oxide nanoparticles: surface tunability for biomedical, sensing and environmental applications. *Nanomaterials*. 2019;9(11):1608. doi:10.3390/nano9111608
11. Izadiyan Z, Shameli K, Miyake M, et al. Green fabrication of biologically active magnetic core-shell Fe_3O_4/Au nanoparticles and their potential anticancer effect. *Mater Sci Eng C*. 2019;96:51–57. doi:10.1016/j.msec.2018.11.008
12. Herlekar M, Barve S, Kumar R. Plant-mediated green synthesis of iron nanoparticles. *J Nanopart*. 2014;2014:1–9. doi:10.1155/2014/140614
13. Reddy LH, Arias JL, Nicolas J, Couvreur P. Magnetic nanoparticles: design and characterization, toxicity and biocompatibility, pharmaceutical and biomedical applications. *Chem Rev*. 2012;112(11):5818–5878. doi:10.1021/cr300068p
14. Kallumadil M, Tada M, Nakagawa T, Abe M, Southern P, Pankhurst QA. Suitability of commercial colloids for magnetic hyperthermia. *J Magn Magn Mater*. 2009;321(10):1509–1513. doi:10.1016/j.jmmm.2009.02.075
15. Ogholbeyg AB, Kianvash A, Hajalilou A, Abouzari-Lotf E, Zarebkohan A. Cytotoxicity characteristics of green assisted-synthesized superparamagnetic maghemite (γ-Fe_2O_3) nanoparticles. *J Mater Sci Mater Electron*. 2018;29(14):12135–12143. doi:10.1007/s10854-018-9321-8
16. Izadiyan Z, Shameli K, Miyake M, et al. Cytotoxicity assay of plant-mediated synthesized iron oxide nanoparticles using Juglans regia green husk extract. *Arab J Chem*. 2018. doi:10.1016/j.arabjc.2018.02.019
17. Tungmunnithum D, Thongboonyou A, Pholboon A, Yangsabai A. Flavonoids and other phenolic compounds from medicinal plants for pharmaceutical and medical aspects: an overview. *Medicines*. 2018;5(3):93. doi:10.3390/medicines5030093
18. Pan-In P, Wanichwecharungruang S, Hanes J, Kim AJ. Cellular trafficking and anticancer activity of *Garcinia mangostana* extract-encapsulated polymeric nanoparticles. *Int J Nanomedicine*. 2014;9:3677. doi:10.2147/IJN.S66511
19. Suttirak W, Manurakchinakorn S. In vitro antioxidant properties of mangosteen peel extract. *J Food Sci Technol*. 2014;51(12):3546–3558. doi:10.1007/s13197-012-0887-5
20. El-Faham S, Mohsen M, Sharaf A, Zaky A. Utilization of mango peels as a source of polyphenolic antioxidants. *Curr Sci Int*. 2016;5(04):529–542.
21. Yew YP, Shameli K, Mohamad SEB, et al. Potential anticancer activity of protocatechuic acid loaded in montmorillonite/Fe_3O_4 nanocomposites stabilized by seaweed Kappaphycus alvarezii. *Int J Pharm*. 2019;572:118743. doi:10.1016/j.ijpharm.2019.118743
22. Yusefi M, Bte Rasit Ali R, Abdullah EC, Shameli K. Analysis on physiochemical properties of cellulose fiber from rice straw waste. *IOP Conf Ser Mater Sci Eng*. 2020;808(1):012038. doi:10.1088/1757-899X/808/1/012038
23. Chaovanalikit A, Mingmuang A, Kitbunluewit T, Choldumrongkool N, Sondee J, Chupratum S. Anthocyanin and total phenolics content of mangosteen and effect of processing on the quality of mangosteen products. *Int Food Res J*. 2012;19(3):1047.
24. Obolskiy D, Pischel I, Siriwatanametanon N, Heinrich M. *Garcinia mangostana* L. a phytochemical and pharmacological review. *Phytother Res*. 2009;23(8):1047–1065. doi:10.1002/ptr.2730
25. Akao Y, Nakagawa Y, Nozawa Y. Anti-cancer effects of xanthones from pericarps of mangosteen. *Int J Mol Sci*. 2008;9(3):355–370. doi:10.3390/ijms9030355
26. Xin Lee K, Shameli K, Miyake M, et al. Green synthesis of gold nanoparticles using aqueous extract of *Garcinia mangostana* fruit peels. *J Nanomater*. 2016;2016:1–7. doi:10.1155/2016/8489094
27. Lee KX, Shameli K, Mohamad SE, et al. Bio-mediated synthesis and characterisation of silver nanocarrier, and its potent anticancer action. *Nanomaterials*. 2019;9(10):1423. doi:10.3390/nano9101423
28. Zahedi-Tabar Z, Bagheri-Khoulenjani S, Amanpour S, Mirzadeh HA. Review on the application of in vitro and in vivo models of cancerous tumors for the study of the hyperthermia effect. *Basic Clin Cancer Res*. 2019. doi:10.18502/bccr.v11i1.1653
29. Hedayatnasab Z, Abnisa F, Daud WMAW. Review on magnetic nanoparticles for magnetic nanofluid hyperthermia application. *Mater Des*. 2017;123:174–196. doi:10.1016/j.matdes.2017.03.036
30. Evans BA, Bausch MD, Sienerth KD, Davern MJ. Non-monotonicity in the influence of nanoparticle concentration on SAR in magnetic nanoparticle hyperthermia. *J Magn Magn Mater*. 2018;465:559–565. doi:10.1016/j.jmmm.2018.06.051
31. Giustini AJ, Petryk AA, Cassim SM, Tate JA, Baker I, Hoopes PJ. Magnetic nanoparticle hyperthermia in cancer treatment. *Nano Life*. 2010;1(01 & 02):17–32. doi:10.1142/S1793984410000067
32. World Health Organization. *WHO Report on Cancer: Setting Priorities, Investing Wisely and Providing Care for All*. 2020.
33. Kumar A, Pandey AK, Singh SS, Shanker R, Dhawan A. Cellular uptake and mutagenic potential of metal oxide nanoparticles in bacterial cells. *Chemosphere*. 2011;83(8):1124–1132. doi:10.1016/j.chemosphere.2011.01.025
34. Jahangirian H, Kalantari K, Izadiyan Z, Rafiee-Moghaddam R, Shameli K, Webster TJ. A review of small molecules and drug delivery applications using gold and iron nanoparticles. *Int J Nanomedicine*. 2019;14:1633–1657. doi:10.2147/IJN.S184723
35. Kumar P, Agnihotri S, Roy I. Preparation and characterization of superparamagnetic iron oxide nanoparticles for magnetically guided drug delivery. *Int J Nanomedicine*. 2018;13(T–NANO2014 Abstracts):43. doi:10.2147/IJN.S125002
36. Gaharwar US, Meena R, Rajamani P. Biodistribution, clearance and morphological alterations of intravenously administered iron oxide nanoparticles in male Wistar rats. *Int J Nanomedicine*. 2019;14:9677. doi:10.2147/IJN.S223142
37. Ahmed MSU, Salam AB, Clayton Yates KW, Jaynes J, Turner T, Abdalla MO. Double-receptor-targeting multifunctional iron oxide nanoparticles drug delivery system for the treatment and imaging of prostate cancer. *Int J Nanomedicine*. 2017;12:6973. doi:10.2147/IJN.S139011

38. Predescu AM, Matei E, Berbecaru AC, et al. Synthesis and characterization of dextran-coated iron oxide nanoparticles. *R Soc Open Sci*. 2018;5(3):171525. doi:10.1098/rsos.171525
39. Xing Y, Jin -Y-Y, Si J-C, et al. Controllable synthesis and characterization of Fe_3O_4/Au composite nanoparticles. *J Magn Magn Mater*. 2015;380:150–156. doi:10.1016/j.jmmm.2014.09.060
40. Izak-Nau E, Huk A, Reidy B, et al. Impact of storage conditions and storage time on silver nanoparticles' physicochemical properties and implications for their biological effects. *RSC Adv*. 2015;5(102): 84172–84185. doi:10.1039/C5RA10187E
41. Nurdin I. The effect of pH and time on the stability of superparamagnetic maghemite nanoparticle suspensions. *MATEC Web Conf*. 2016;39:01001. doi:10.1051/matecconf/20163901001
42. Dabbagh A, Hedayatnasab Z, Karimian H, et al. Polyethylene glycol-coated porous magnetic nanoparticles for targeted delivery of chemotherapeutics under magnetic hyperthermia condition. *Int J Hyperth*. 2019;36(1):104–114. doi:10.1080/02656736.2018.1536809
43. Chiriac H, Petreus T, Carasevici E, et al. In vitro cytotoxicity of Fe–Cr–Nb–B magnetic nanoparticles under high frequency electromagnetic field. *J Magn Magn*. 2015;380:13–19. doi:10.1016/j.jmmm.2014.10.015
44. Hedayatnasab Z, Dabbagh A, Abnisa F, Daud WMAW. Polycaprolactone-coated superparamagnetic iron oxide nanoparticles for in vitro magnetic hyperthermia therapy of cancer. *Eur Polym J*. 2020;133:109789. doi:10.1080/02656736.2018.1536809
45. Hedayatnasab Z, Dabbagh A, Abnisa F, Daud WMAW. Synthesis and in-vitro characterization of superparamagnetic iron oxide nanoparticles using a sole precursor for hyperthermia therapy. *Mater Res Bull*. 2020;132:110975. doi:10.1016/j.materresbull.2020.110975
46. Yew YP, Shameli K, Mohamad SE, Lee KX, Teow S-Y. Green synthesized montmorillonite/carrageenan/Fe_3O_4 nanocomposites for ph-responsive release of protocatechuic acid and its anticancer activity. *Int J Mol Sci*. 2020;21(14):4851. doi:10.3390/ijms21144851
47. Yusefi M, Shameli K, Jahangirian H, et al. The potential anticancer activity of 5-fluorouracil loaded in cellulose fibers isolated from rice straw. *Int J Nanomedicine*. 2020;15:5417–5432. doi:10.2147/IJN.S250047
48. Holzwarth U, Gibson N. The Scherrer equation versus the 'Debye-Scherrer equation'. *Nat Nanotechnol*. 2011;6(9):534. doi:10.1038/nnano.2011.145
49. Kroon R. Nanoscience and the Scherrer equation versus the Scherrer-Gottingen equation. *S Afr J Sci*. 2013;109(5–6):01–02. doi:10.1590/sajs.2013/a0019
50. van Ommen JR, Valverde JM, Pfeffer R. Fluidization of nanopowders: a review. *J Nanopart Res*. 2012;14(3):737. doi:10.1007/s11051-012-0737-4
51. Amemiya Y, Arakaki A, Staniland SS, Tanaka T, Matsunaga T. Controlled formation of magnetite crystal by partial oxidation of ferrous hydroxide in the presence of recombinant magnetotactic bacterial protein Mms6. *Biomaterials*. 2007;28(35):5381–5389. doi:10.1016/j.biomaterials.2007.07.051
52. Yang J, Kim J, Lee J, et al. Inverted hysteresis loops observed in a randomly distributed cobalt nanoparticle system. *Phys Rev B*. 2008;78(9):094415. doi:10.1103/PhysRevB.78.094415
53. Rohman A, Arifah FH, Irnawati GA, Muchtaridi M. The application of FTIR spectroscopy and chemometrics for classification of mangosteen extract and its correlation with alpha-mangostin. *J Appl Pharm*. 2020;10(04):149–154. doi:10.7324/JAPS.2020.104019
54. Li G, Petiwala SM, Yan M, Won JH, Petukhov PA, Johnson JJ. Gartanin, an isoprenylated xanthone from the mangosteen fruit (*Garcinia mangostana)*, is an androgen receptor degradation enhancer. *Mol Nutr Food Res*. 2016;60(6):1458–1469. doi:10.1002/mnfr.201600037
55. Demir A, Topkaya R, Baykal A. Green synthesis of superparamagnetic Fe_3O_4 nanoparticles with maltose: its magnetic investigation. *Polyhedron*. 2013;65:282–287. doi:10.1016/j.poly.2013.08.041
56. Testa-Anta M, Ramos-Docampo MA, Comesaña-Hermo M, Rivas-Murias B, Salgueiriño V. Raman spectroscopy to unravel the magnetic properties of iron oxide nanocrystals for bio-related applications. *Nanoscale Adv*. 2019;1(6):2086–2103. doi:10.1039/C9NA00064J
57. Sathishkumar G, Logeshwaran V, Sarathbabu S, et al. Green synthesis of magnetic Fe_3O_4 nanoparticles using *Couroupita guianensis* Aubl. fruit extract for their antibacterial and cytotoxicity activities. *Artif Cell Nanomed*. 2018;46(3):589–598. doi:10.1080/21691401.2017.1332635
58. Durán J, Arias J, Gallardo V, Delgado A. Magnetic colloids as drug vehicles. *J Pharm Sci*. 2008;97(8):2948–2983. doi:10.1002/jps.21249
59. Zaloga J, Janko C, Agarwal R, et al. Different storage conditions influence biocompatibility and physicochemical properties of iron oxide nanoparticles. *Int J Mol Sci*. 2015;16(5):9368–9384. doi:10.3390/ijms16059368
60. Kerroum MA, Essyed A, Iacovita C, et al. The effect of basic pH on the elaboration of $ZnFe_2O_4$ nanoparticles by co-precipitation method: structural, magnetic and hyperthermia characterization. *J Magn Magn Mater*. 2019;478:239–246. doi:10.1016/j.jmmm.2019.01.081
61. Yew YP, Shameli K, Miyake M, et al. Green synthesis of magnetite (Fe_3O_4) nanoparticles using seaweed (*Kappaphycus alvarezii*) extract. *Nanoscale Res Lett*. 2016;11(1):276. doi:10.1186/s11671-016-1498-2
62. Widowati W, Darsono L, Suherman J, Yelliantty Y, Maesaroh M. High performance liquid chromatography (HPLC) analysis, antioxidant, anti-aggregation of mangosteen peel extract (*Garcinia mangostana* L.). *IJBBB*. 2014;4(6):458. doi:10.17706/ijbbb.2014.4.6.458-466
63. Singh N, Jenkins GJ, Asadi R, Doak SH. Potential toxicity of superparamagnetic iron oxide nanoparticles (SPION). *Nano Rev*. 2010;1(1):5358. doi:10.3402/nano.v1i0.535
64. Ciocca DM, Calderwood SK. Heat shock proteins in cancer: diagnostic, prognostic, predictive, and treatment implications 70. *Cell Stress Chaperones*. 2005;10(2):86–103. doi:10.1379/CSC-99r.1